Theory of modulated phases in lipid bilayers and liquid crystal films

C.-M. Chen and F. C. MacKintosh

Department of Physics, University of Michigan, Ann Arbor, Michigan 48109-1120

(Received 5 September 1995)

We present a general theory for equilibrium-modulated phases of chiral and achiral bilayer membranes and liquid crystal films. Both bulk smectics as well as freely suspended films are considered. For flexoelectric systems, continuous structural phase transitions are predicted among square-lattice, hexagonal, and distorted two-dimensional modulated phases as a function of the applied electric field. It is also shown that only uniform flat phases are predicted for thin films. One-dimensional ripple phases and two-dimensional square-lattice phases can occur with increasing film thickness. [S1063-651X(96)03205-9]

PACS number(s): 61.30.Cz, 64.60.−i, 64.70.Md

I. INTRODUCTION

The study of two-dimensional surfaces is an important subject in both physics and biology. In many ways, lipid bilayer membranes provide experimental realization of random surfaces and excellent model systems of cell membranes. These membranes are composed of amphiphilic molecules which have charged or polar heads and one or two hydrocarbon tails. When these molecules are dissolved in water at sufficient concentration, they self-assemble into bilayer membranes in which their hydrophobic tails are shielded from contact with the surrounding water. Under appropriate conditions, lamellar phases consisting of periodically spaced parallel membranes separated by water are the equilibrium phases. Membranes in lamellar phases as well as isolated membranes (e.g., in closed vesicles) can exhibit varying degrees of in-plane order. Above the chain-melting temperature, the membranes form an equilibrium L_α lamellar phase in which the long axes of constituent molecules are on average parallel to the membrane normal. This phase has the same symmetry as the liquid crystalline smectic-A phase. At low temperatures, the membranes develop molecular tilt relative to the membrane normal. In this $L_{\beta'}$ phase, the tilt orientational order is similar to the liquid crystalline smectic-C phase. However the $L_{\beta'}$ phase also exhibits bond orientational order [1]. In fact, three distinct hexatic phases have been reported in this region. For a number of lipids with saturated acyl chains, such as dimyristoyl phosphatidylcholine (DMPC), in addition to the tilted $L_{\beta'}$ phase, a modulated $P_{\beta'}$ phase is observed in the hydrated lamellar systems. This phase is characterized by a one-dimensional height modulation of each membrane [1–6] in addition to a nonzero molecular tilt [2,3]. Such a structure thus exhibits broken translation invariance in one of the in-plane directions within each membrane [7].

Similar to lipid bilayer membranes, liquid crystal films also exhibit a number of thermodynamically distinct phases, including various modulated phases that result from competing interactions. For instance, chiral smectic liquid crystal films and lyotropic lamellar phases have been shown to form various striped modulated phases [1,2,8,9]. A similar striped domain phase due to the surface polarization asymmetry has also been seen in achiral films [10,11]. Furthermore, theories

predict hexagonal modulated phases in strongly chiral thermotropic films [12]. Although these hexagonal phases have apparently not yet been observed experimentally, experiments with freely suspended liquid crystal films have demonstrated more than one square-lattice modulated phase [13]. In addition to these square-lattice modulated phases, the films studied in Ref. [13] showed one-dimensional modulated phases similar to the $P_{\beta'}$ phases of lipid bilayers, as well as a number of uniform smectic phases with varying degrees of in-plane orientational order. Such freely suspended smectic liquid crystal films are also attractive systems for the study of two-dimensional surfaces. Uniform, stable, large-area (10 cm^2) films can be made which consist of only two molecular layers ($N=2$). Moreover, the film thickness can be increased to study the evolution to three dimensions. Various techniques including x-ray scattering have been applied to study the intermolecular correlations and phase transitions in the various smectic phases. A schematic representation of the phase diagram for 4-n-heptyloxybenzylidene-4-n-heptylaniline (7O.7) [13] obtained from x-ray scattering for varying temperature and number of layers is shown in Fig. 1.

In this paper, we present and analyze a phenomenological Landau model [14–16] for tilted bilayer membranes that includes coupling between tangent plane order and membrane shape (or curvature) and chiral couplings present when constituent molecules are chiral. This model is applicable to both classes of membranes described above. This model predicts the existence of a number of distinct rippled phases distinguished by height profiles of different symmetry and by different tilt-order-parameter configurations relative to the ripples. Finally, the model predicts the existence of phases with two-dimensional rather than one-dimensional height modulations.

In the following section, we will present our phenomenological model for both chiral and achiral membranes. In Sec. III, we will study the effect of an applied electric field on achiral membranes. A numerical approach and results from this model will be discussed in Sec. IV. In Sec. V, we will illustrate the effect of the confinement of a smectic domain confined between walls. Finally, we will give a detailed analysis for the phase diagrams in freely suspended films and compare the experimental results with ours.
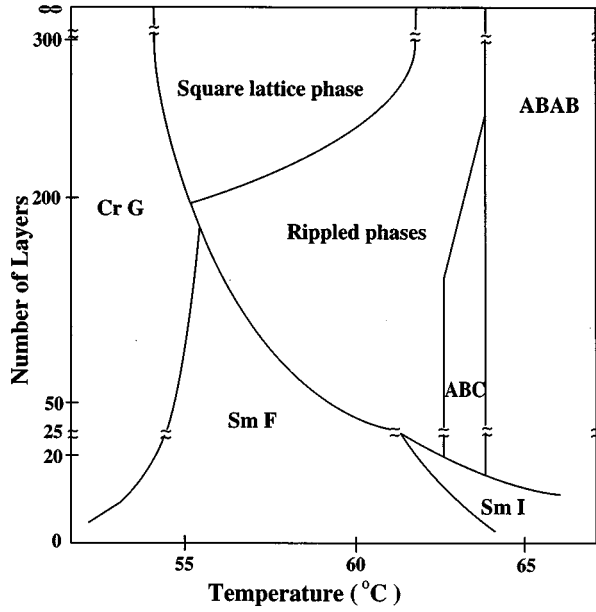
FIG. 1. The phase diagram of 7O.7 as a function of the temperature and number-of-layers (N), showing the square-lattice phase, one-dimensional rippled phases, and several uniform flat phases. The square-lattice phase occurs for the number of layers greater than 200 and for temperatures between 55 °C and 62 °C.

II. THE MODEL

In previous papers [14–16], we have developed a phenomenological Landau theory for molecular tilt and membrane shape. This model was used to explain the possible origin of the one-dimensional modulated $P_{\beta'}$ phase in lipid bilayers, as well as the shape of the chiral stripe phases that can result from the coupling of the molecular tilt to the membrane curvature. In this paper, we focus primarily on possible two-dimensional phases of lipid bilayers and liquid crystal films. The latter have been shown to form such two-dimensional modulated phases with square symmetry [13]. These square-lattice phases, however, have only been observed for thick films of more than approximately 200 layers. Thus we have also extended our previous work to the case of freely suspended films of finite thickness. Furthermore, in order to elucidate the origin of these square-lattice phases and the possibility of other structures, such as hexagonal phases, we have examined the effect of the symmetry breaking fields, such as an applied electric field perpendicular to the film. We find a sequence of structural phase transitions in such films, in which, as a function of the applied field, the square-lattice phase evolves continuously into a splay hexagonal phase with a distinct intermediate phase of lower symmetry.

The molecular orientation can be determined by the projection $\mathbf{m}$ of the local director $\mathbf{n}$ onto the local tangent plane to the membrane, as depicted schematically in Fig. 2. We include the coupling of the molecular tilt to the membrane curvature. This coupling results from steric interactions between neighboring molecules. A divergence of $\mathbf{m}$ corresponds to a varying tilt angle of the molecules relative to the surface, which gives rise to a *spontaneous curvature* of the membrane. The model free energy is given by
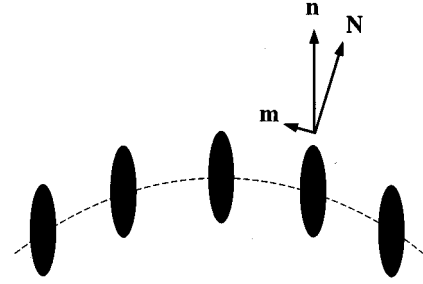

FIG. 2. Smectic-C order within a liquid crystal film or lipid bilayer membrane arises from a tilt of the constituent molecules (represented by the solid oval and unit director $\mathbf{n}$). In the case of a curved membrane, the orientation is defined with respect to the neighboring molecules. Equivalently, the tilt is characterized relative to the local normal $\mathbf{N}$ to the membrane. The surface component $\mathbf{m} = \mathbf{n} - (\mathbf{N} \cdot \mathbf{n})\mathbf{N}$ represents a two-dimensional vector order parameter.

$$f = f_{\mathbf{m}} + f_{\text{bend}}, \tag{1}$$

where

$$f_{\mathbf{m}} = \tfrac{1}{2} C_{\|} (\boldsymbol{\nabla} \cdot \mathbf{m})^2 + \tfrac{1}{2} C_{\perp} (\boldsymbol{\nabla} \times \mathbf{m})^2 + \tfrac{1}{2} D (\nabla^2 \mathbf{m})^2$$
$$+ \tfrac{1}{2} t |\mathbf{m}|^2 + u |\mathbf{m}|^4, \tag{2}$$

and

$$f_{\text{bend}} = \frac{1}{2} \kappa (\nabla^2 h)^2 - \gamma (\nabla^2 h)(\boldsymbol{\nabla} \cdot \mathbf{m}). \tag{3}$$

Here $h(x,y)$ is the height of the membrane relative to some flat plane with coordinates (x,y), and $\nabla_i \nabla_j h(x,y)$ is the linearized curvature tensor. The equilibrium membrane shape is given by

$$\nabla^2 h = \frac{\gamma}{\kappa} (\boldsymbol{\nabla} \cdot \mathbf{m}). \tag{4}$$

When h is replaced by this equilibrium value, we obtain the effective free energy as given by

$$f = \tfrac{1}{2} C_{\|}' (\boldsymbol{\nabla} \cdot \mathbf{m})^2 + \tfrac{1}{2} C_{\perp} (\boldsymbol{\nabla} \times \mathbf{m})^2$$
$$+ \tfrac{1}{2} D (\nabla^2 \mathbf{m})^2 + \tfrac{1}{2} t |\mathbf{m}|^2 + u |\mathbf{m}|^4, \tag{5}$$

with a reduced longitudinal elastic constant $C_{\|}' = C_{\|} - \gamma^2/\kappa$. When $C_{\|}' > 0$, the equilibrium phases are spatially uniform; when $C_{\|}' < 0$, modulated phases are possible with a characteristic wave number $q_0 = (2\pi/\lambda) = \sqrt{|C_{\|}'|/2D}$ that tends to zero at $C_{\|}' = 0$.

Several one-dimensional modulated phases of this model were examined previously [14,15]. A square-lattice phase also occurs for the model in Eq. (5). The structure is sketched in Fig. 3(a). In terms of the molecular orientation, this phase can be characterized as a vortex-antivortex phase, with two strength $+1$ vortices located at two corners of the unit cell and two strength -1 vortices located at the other corners.

In chiral membranes, since chiral molecules have no inversion symmetry, additional chiral terms must be included
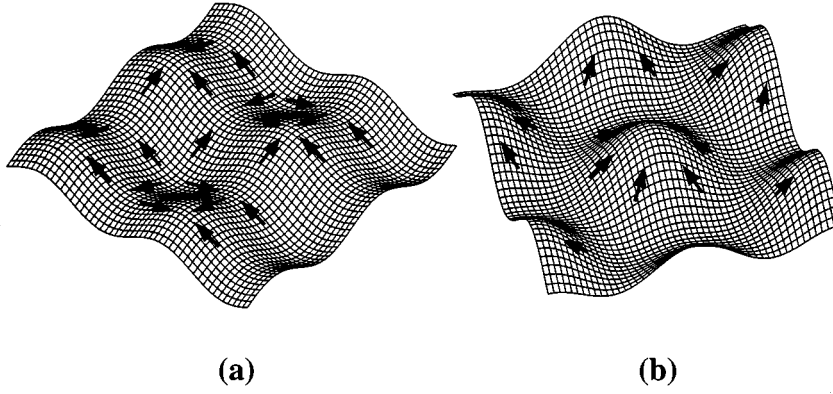
FIG. 3. A representation of the membrane shape and the tilt field $\mathbf{m}$ in the two-dimensional modulated phases: (a) the square-lattice phase and (b) the splay hexagonal phase. Note that the square-lattice phase maintains an inversion symmetry of the film. This symmetry is not present in (b).

(a)   **(b)**

in Eq. (5). By symmetry, the lowest-order chiral coupling for a bilayer is $|\mathbf{m}|^2(\boldsymbol{\nabla}\times\mathbf{m})$ [12,17,18]. So, the effective free energy for chiral membranes becomes

$$f_{ch}=\tfrac{1}{2}C'_{\parallel}(\boldsymbol{\nabla}\cdot\mathbf{m})^2+\tfrac{1}{2}C_{\perp}(\boldsymbol{\nabla}\times\mathbf{m})^2+\tfrac{1}{2}D(\nabla^2\mathbf{m})^2+\tfrac{1}{2}t|\mathbf{m}|^2$$
$$+u|\mathbf{m}|^4+\lambda_b|\mathbf{m}|^2(\boldsymbol{\nabla}\times\mathbf{m}). \tag{6}$$

A coupling of tilt and shape $\epsilon_{ki}(\nabla_i\nabla_j h)m_j m_k$ is also possible [19] in chiral membranes. However, to this order, its effect is the same as the last term in Eq. (6) [15]. The chiral term above lowers the symmetry of rippled phases and also leads to additional chiral phases, such as the chiral stripe phase and hexagonal phase of Refs. [12,20]. The appearance of these modulated chiral phases is due to the fact that the chiral term will effectively reduce the bend elastic constant $C_{\perp}$, leading to an instability of the flat membrane. Therefore for λ_b greater than a critical value $\sqrt{2uC_{\perp}}$, the equilibrium phase is the bend stripe phase of Ref. [20]. Although it is characterized primarily by bend, this phase also exhibits a splay modulation, i.e., $\boldsymbol{\nabla}\cdot\mathbf{m}\neq0$. As a result of the coupling between splay and curvature in Eq. (3), this phase also exhibits a ripple structure. As is described in Ref. [15], the shape of this bend stripe phase can be obtained from Eq. (4).

III. THE EFFECT OF AN APPLIED ELECTRIC FIELD

For systems with lower symmetry, additional phases are possible. For example, lipid monolayers at the air-water interface do not maintain the up-down symmetry. The lack of up-down symmetry can lead to new phases. One example of a *continuously variable* symmetry breaking field is an electric field applied parallel to the layer normal. For flexoelectric systems [17,21–24], we show that such an applied electric field can be used to study structural phase transitions, including the evolution of square-lattice phases such as those of Ref. [13] to possible hexagonal modulated phases.

Consider a smectic-A layer parallel to the x-y plane in the presence of an applied electric field $\mathbf{E}$. The lowest-order coupling of the molecular tilt to the field is [17,21]

$$-e_1\mathbf{E}\cdot\hat{\mathbf{n}}(\boldsymbol{\nabla}\cdot\hat{\mathbf{n}}), \tag{7}$$

where $\hat{\mathbf{n}}\cong(1-\tfrac{1}{2}m^2)\hat{\mathbf{z}}+\mathbf{m}$ is the director, $\mathbf{m}$ is the projection of the molecular tilt in the x-y plane, and e_1 is the flexoelectric coefficient. The typical values of e_1 in thermotropic liquid crystals are in the range of 10^{-4} esu/cm [24]. For an applied field along the z axis, this coupling gives two terms: $-e_1E_z(\boldsymbol{\nabla}\cdot\mathbf{m})$, which is a total derivative, and $e_1E_zm^2(\boldsymbol{\nabla}\cdot\mathbf{m})$. Therefore the free energy of a membrane in the presence of an applied electric field along the z axis can be expressed as

$$f_E=\tfrac{1}{2}C'_{\parallel}(\boldsymbol{\nabla}\cdot\mathbf{m})^2+\tfrac{1}{2}C_{\perp}(\boldsymbol{\nabla}\times\mathbf{m})^2+\tfrac{1}{2}D(\nabla^2\mathbf{m})^2+\tfrac{1}{2}t|\mathbf{m}|^2$$
$$+u|\mathbf{m}|^4+\lambda_s|\mathbf{m}|^2(\boldsymbol{\nabla}\cdot\mathbf{m}), \tag{8}$$

where the splay coupling constant $\lambda_s=e_1aE_z$ and a is the average layer spacing. This model is also formally similar to that of Refs. [12,20] for chiral smectic-C^* films. In particular, for ferroelectrics, the polarization vector $\mathbf{P}\sim\mathbf{N}\times\mathbf{n}$ is perpendicular to $\mathbf{m}$ above. For such systems, the model in terms of the polarization $\mathbf{P}$ is similar to Eq. (8) with $\mathbf{m}$ replaced by $\mathbf{P}$ [20]. These models of smectic-C^* films predict bend hexagonal phases that differ from the modulated phases considered here in that they involve bend rather than splay.

This coupling can be understood within a simple picture due to Meyer [21] for molecules with both a permanent electric dipole and a shape asymmetry (under $\mathbf{n}\rightarrow-\mathbf{n}$). For such a system, a splay of the molecules in a nematic or a smectic phase leads to an electric polarization. For strong shape asymmetry, the coupling coefficient, which has units of electric charge per length, is expected to be of the order μ/d^2, where μ is the electric dipole and d is the size of the molecules [17]. It has also been shown that a quadrupolar model [22,23] leads to a flexoelectric coupling of the same magnitude, even for symmetric molecules. This is consistent with the experimental observation that a wide variety of systems ranging from symmetric to highly asymmetric molecules have a very similar coupling coefficient e_1 in the range of 10^{-4} esu/cm [24].

For lyotropic systems, this coupling can also be understood as the modification of the dipole-dipole interaction within a bilayer in the presence of an applied electric field along the z axis, provided that the head groups have a permanent dipole moment. The splay coupling constant λ_s above can be estimated by calculating the dipole-dipole interaction energy. As shown in Fig. 4, the dipole moment p_i of each molecule under the electric field of strength E is expressed as

$$p_i=\mu+\alpha E_z\cos(\theta_i)=\mu+\alpha E_z(1-\tfrac{1}{2}m_i^2), \tag{9}$$
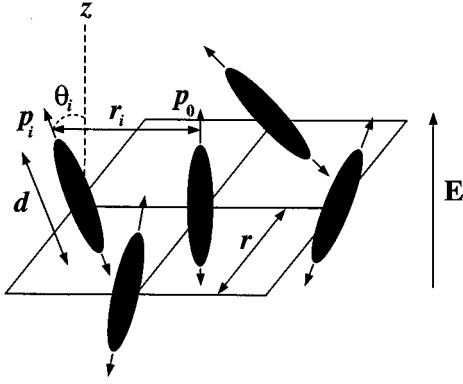
FIG. 4. A schematic representation of the dipole-dipole interaction of a bilayer membrane in a unit cell in the presence of an applied electric field along the z axis. p_i and θ_i denote the dipole moment and orientation of each molecule, respectively.

where θ_i is the dipole orientation of each molecule and α is the molecular polarizability. Considering only nearest-neighbor interaction, the dipole-dipole interaction energy per unit area for the upper layer is

$$H_{dd} = \frac{1}{\epsilon r^2} \sum_{i=1}^{4} \frac{\mathbf{p}_0 \cdot \mathbf{p}_i - 3(\hat{\mathbf{r}}_i \cdot \mathbf{p}_0)(\hat{\mathbf{r}}_i \cdot \mathbf{p}_i)}{\mathbf{r}_i^3}, \tag{10}$$

where $\mathbf{r}_i$ is the distance from the central dipole to the ith dipole and r is the distance between two neighboring molecules. Including the contribution from the lower layer, the splay chiral term in Eq. (10) is found to be

$$f_s = \frac{48 d \alpha \mu E_z}{\epsilon r^5} |\mathbf{m}|^2 (\boldsymbol{\nabla} \cdot \mathbf{m}). \tag{11}$$

Therefore we obtain the splay chiral coupling constant as

$$\lambda_s = \frac{48 d \alpha \mu E_z}{\epsilon r^5}. \tag{12}$$

The above bilayer dimensions can be determined definitively by x-ray diffraction [25]. Typical values for phospholipid bilayers are $r^2 \sim 40$ Å^2 and $d \sim 30$ Å. The permanent dipole moment μ has been suggested to be 20 debye [26,27]. The dielectric constant ϵ of water is about 80. Finally, the molecular polarizability includes electronic polarizability and orientational polarizability. A theoretical estimation gives $\alpha \sim 10$ Å^3. Correspondingly, for lyotropic systems, the flexoelectric coefficient e_1 is also of order 10^{-4} esu/cm.

IV. NUMERICAL APPROACH AND RESULTS

To determine the mean-field phase diagram, we numerically minimize the free energy in Eqs. (6) and (8) in which the order parameter is represented by its Fourier series in two-dimensional $\mathbf{k}$ space. The general form of the free energy in $\mathbf{k}$ space is
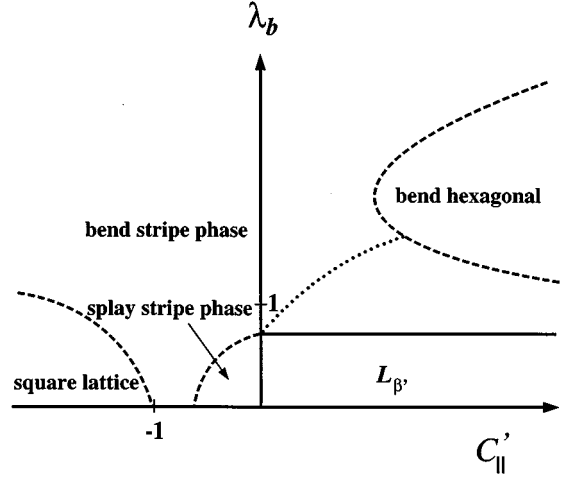

FIG. 5. The mean-field phase diagram of the chiral membranes as a function of $C_{\parallel}'$ and λ_b for $C_{\perp} = 0.2$ and $t = -1.5$. The bend stripe phase is favored at a large chirality and the bend hexagonal phase is favored at large asymmetry, $\Delta = C_{\parallel}' - C_{\perp}$. In the region of positive $C_{\parallel}'$, the dotted line distinguishes two regions with different topological winding numbers 0 or 1. The solid line indicates a second-order transition, while the dashed lines indicate first-order transitions. The units of length and energy are 100 Å and 10^{-12} erg, respectively.

$$\langle f_E \rangle \equiv \frac{\iint f_E dx dy}{\iint dx dy}$$

$$= \sum_{\mathbf{k}} \frac{1}{2} \{ C_{\parallel}' |k_x a_{\mathbf{k}} + k_y b_{\mathbf{k}}|^2 + C_{\perp} |k_x b_{\mathbf{k}} - k_y a_{\mathbf{k}}|^2$$

$$+ [D(k_x^2 + k_y^2)^2 + t](|a_{\mathbf{k}}|^2 + |b_{\mathbf{k}}|^2) \}$$

$$+ \sum_{\mathbf{k}_1, \mathbf{k}_2, \mathbf{k}_3} u \{ a_{\mathbf{k}_1} a_{\mathbf{k}_2} a_{\mathbf{k}_3} a_{\mathbf{k}_4} + b_{\mathbf{k}_1} b_{\mathbf{k}_2} b_{\mathbf{k}_3} b_{\mathbf{k}_4}$$

$$+ 2 a_{\mathbf{k}_1} a_{\mathbf{k}_2} b_{\mathbf{k}_3} b_{\mathbf{k}_4} \} + \sum_{\mathbf{k}, \mathbf{k}'} \lambda_b \{ (a_{\mathbf{k}} a_{\mathbf{k}'} + b_{\mathbf{k}} b_{\mathbf{k}'})(k_x'' b_{\mathbf{k}'}$$

$$- k_y'' a_{\mathbf{k}'}) \} + \sum_{\mathbf{k}, \mathbf{k}'} \lambda_s \{ (a_{\mathbf{k}} a_{\mathbf{k}'} + b_{\mathbf{k}} b_{\mathbf{k}'})(k_x'' a_{\mathbf{k}'} + k_y'' b_{\mathbf{k}'}) \},$$

$$\tag{13}$$

where $a_{\mathbf{k}}$ and $b_{\mathbf{k}}$ are the corresponding complex coefficients of the Fourier expansion of m_x and m_y, $\mathbf{k}_4 = -\mathbf{k}_1 - \mathbf{k}_2 - \mathbf{k}_3$, $\mathbf{k}'' = -\mathbf{k} - \mathbf{k}'$, $k_x = mq_1 + nq_2$, and $k_y = nq_3$ for any integers m, n. To find the ground state of this free energy, we can numerically minimize Eq. (13) in a multidimensional space of amplitudes $\{a_{\mathbf{k}}, b_{\mathbf{k}}\}$. In addition, we consider variable basis vectors of the reciprocal space, $(q_1, 0)$ and (q_2, q_3). A combination of simulated annealing and conjugate gradient minimization was employed to find the ground state for the system. This combination effectively improved the speed in searching for the ground state over simulated annealing alone.

The phase diagram of chiral membranes for $C_{\perp} = 0.2$ and $t = -1.5$ is shown in Fig. 5. As was found analytically in Refs. [14,15], in this phase diagram, at zero chirality, we
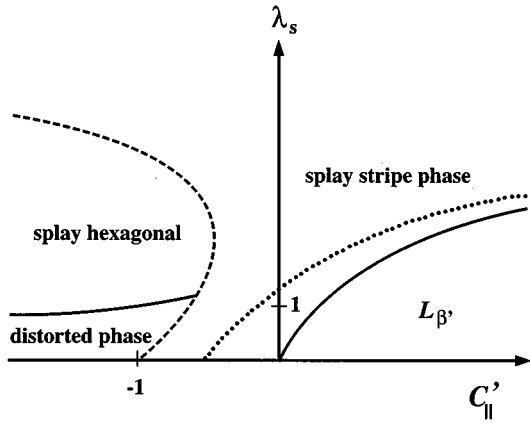
FIG. 6. The mean-field phase diagram of the achiral membranes as a function of $C_\parallel'$ and λ_s for $C_\perp = 0.2$ and $t = -1.5$. λ_s is proportional to the applied electric field E. The solid lines indicate the second-order transitions, while the dashed lines indicate the first-order transitions. The dotted line distinguishes two regions with different topological winding numbers 0 or 1. For the zero field, only three phases occur: (i) the $L_{\beta'}$ phase; (ii) the splay stripe phase; and (iii) the square-lattice phase. For the nonzero electric field, the latter distorts continuously to become the "distorted phase" illustrated in Fig. 7(b). Thus a continuous evolution from the square-lattice phase to the splay hexagonal phase is predicted in the region of negative $C_\parallel'$. The units of length and energy are 100 Å and 10^{-12} erg, respectively.

have $L_{\beta'}$, $P_{\beta'}^{(1)}$, $P_{\beta'}^{(3)}$, and the square-lattice phase along the $C_\parallel'$ axis. (We retain the notation for the various one-dimensional modulated phases in Refs. [14,15].) For chiral systems ($\lambda_b \neq 0$), the symmetries of the $L_{\beta'}$ phase and the square-lattice phase are the same, while the symmetries of the $P_{\beta'}^{(1)}$ and $P_{\beta'}^{(3)}$ phases are changed. The resulting one-dimensional ripple phases are a splay stripe phase and a bend stripe phase, respectively. In the region of negative $C_\parallel'$, since the chiral term tends to favor bend, the splay stripe and square-lattice phases eventually become unstable as λ_b increases. On the other hand, the bend stripe phase is favored by this chiral term. Therefore both the splay stripe phase and the square-lattice phase give away to the bend stripe phase at a large chirality. In the region of the positive $C_\parallel'$, the $L_{\beta'}$ phase becomes unstable to the bend stripe phase for $\lambda_b > \sqrt{2uC_\perp}$. This bend stripe phase, as mentioned in Sec. II, is similar to the chiral stripe phase observed in smectic-C^* films. It is interesting to note that the dotted line in the region of the bend stripe phase distinguishes two regions with the same symmetry but different topological winding numbers of the order parameter. The bend stripe phase originating from $P_{\beta'}^{(3)}$ has a winding number 1, while the one originating from $L_{\beta'}$ has a winding number 0. This phenomenon can happen in the absence of D in our model, i.e., for the model considered in Ref. [20]. However, such a model is unstable at large chirality. Since $\sqrt{2uC_\perp}$ is independent of $C_\parallel'$, the phase boundary between $L_{\beta'}$ and the bend stripe phase is a horizontal line in the $C_\parallel'$-λ_b phase diagram. There is also a bend hexagonal phase observed in this region. This result is consistent with the results of Refs. [12,20].

In Fig. 5 the stripe phases are one-dimensional ripples, while the square-lattice phase has a two-dimensional modu-

lated structure. The height profile of the bend hexagonal phase is essentially flat because the source term for the curvature in Eq. (4) is approximately zero. However the tilt field of this phase displays a nontrivial hexagonal structure. As in Ref. [20], we define the asymmetry between splay and bend elastic constants by $\Delta = C_\parallel' - C_\perp$. Our results from the numerical calculations are consistent with Refs. [12,20] in that the bend hexagonal phase is favored at large asymmetry. However the bend hexagonal phase becomes unstable for large chirality, and the bend stripe phase appears. Therefore the competition between chirality and asymmetry Δ determines the phase boundary between the bend stripe phase and the bend hexagonal phase.

In Fig. 6, we plot the phase diagram for the model in Eq. (8) as a function of $C_\parallel'$ and λ_s. At zero electric field, the $L_{\beta'}$ phase is stable in the region of the positive $C_\parallel'$. With a nonzero field, the $L_{\beta'}$ phase is destabilized due to the presence of $|\mathbf{m}|^2 (\nabla \cdot \mathbf{m})$ term which favors splay. Therefore there is a transition from the $L_{\beta'}$ phase to the splay stripe phase for $\lambda_s > \sqrt{2uC_\parallel'}$. We note that this splay stripe phase has the same symmetry as the splay domain phase proposed by Meyer and Pershan [11]. However, our splay stripe phase is expected to exist over a wide range of temperatures for thin films of smectic-C because there are no disclination lines in our case. An estimation of the critical field strength for the induced splay stripe phase gives $E \approx 10^4 - 10^5$ V/cm. In the region of negative $C_\parallel'$, there is a two-dimensional modulated square-lattice phase at zero electric field. The square-lattice phase possesses C_4 and reflection symmetry. The corresponding configuration of the tilt order parameter is shown in Fig. 7(a). For a nonzero electric field, the symmetry of the square-lattice phase is reduced. The in-plane symmetry group is C_2, and the system is no longer symmetric under reflections through the average plane of the membrane. The electric field tends to favor one $+1$ vortex over the other. In other words, the hills in Fig. 3(a) are favored over the valleys. With increasing electric field strength, the disfavored strength $+1$ vortex elongates to become two strength $+1$ vortices and one -1 vortex. As the field strength increases further, the distorted vortex phase becomes the splay hexagonal phase shown in Figs. 3(b) and 7(c). The symmetry group of the splay hexagonal phase is C_6. For the increasing $C_\perp / C_\parallel'$, the phase boundary (dashed line) of this region in Fig. 6 will be shifted toward the region of positive $C_\parallel'$. Therefore for sufficiently large $C_\perp$, the splay hexagonal phase can exist in the region of the positive $C_\parallel'$. This agrees with the results of Jacobs, Goldner, and Mukamel [20].

We note that the evolution from the square-lattice phase to the splay hexagonal phase is a *continuous* process. This evolution of the membrane structure from square-lattice phase to splay hexagonal phase therefore involves two successive second-order structural phase transitions instead of one first-order structural reconstruction. We estimate that the critical field strength for the transition to the splay hexagonal phase is of order $E \approx 10^5 - 10^6$ V/cm. However depending on the material parameters, it could be significantly lower. In any case, for thin film systems such as those studied in Ref. [13], we expect that the square-lattice phase will become a skewed two-dimensional modulated phase for any nonzero applied electric field perpendicular to the layers.

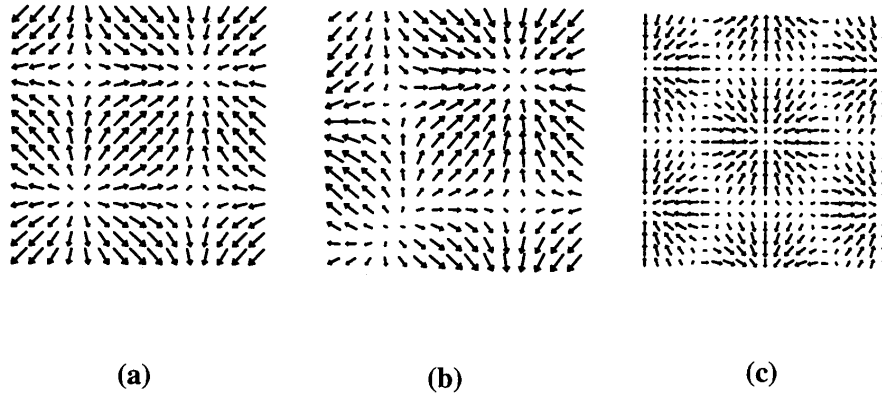**(a)**   **(b)**   **(c)**

FIG. 7. A continuous evolution of the tilt field from the square-lattice phase to the splay hexagonal phase. In the absence of an applied field, the equilibrium phase exhibits a perfect square lattice (a), and inversion symmetry as shown in Fig. 3(a). The symmetry group is C_4, corresponding to the four-fold rotations in the plane of the film. For the nonzero applied field, the structure distorts as shown in (b). The symmetry group is C_2. Also, the inversion symmetry of the film is broken. Above a critical field strength, the film exhibits a six-fold symmetry (C_6) in (c). Here the scale has been somewhat reduced from that of (a) and (b) in order to show the structure of the splay hexagonal phase.

V. CONFINEMENT OF A SMECTIC DOMAIN

In the previous sections, we have given a detailed study of the two-dimensional free membranes. These results are also applicable to three-dimensional lamellar systems in which the boundary effect can be neglected. However for a lamellar system of finite thickness, the boundary effect plays an important role. For example, the surface tension in freely suspended films will tend to suppress the modulated phases. Therefore we extend our study from two-dimensional free membranes to three-dimensional lamellar systems with nonvanishing boundary effects. This analysis is particularly important in understanding the results from experiments of freely suspended films. As an illustration of the boundary effects, we consider the case of a smectic domain confined between walls. The smectic domain is characterized by a stack of parallel membranes equally spaced in the direction perpendicular to the individual sheets. This defines the z direction. Thus the membranes are parallel to the x-y plane. As shown in Fig. 8, the confinement tends to suppress all modulated phases since the undulation of membranes must vanish at both boundaries. In this case, the phase diagrams will approximate those of aligned bulk systems. The undulation of membranes can be described by the local displacement field $u(x,y,z)$, which represents the vertical displacement of a membrane at (x,y,z) away from its average height (z). The elastic energy of distortions per unit volume can be described in terms of gradients of $u(x,y,z)$ [17]

$$f_{\text{bulk}} = \frac{1}{2}K(\nabla^2 u)^2 + \frac{1}{2}\bar{B}\left(\frac{\partial u}{\partial z}\right)^2, \qquad (14)$$

where $K = \kappa/a$. The first term represents the curvature energy of the membranes at (x,y,z), while the second term represents the compression energy of the stack. The phenomenological coupling of the curvature to the molecular tilt becomes

$$f_\gamma = -\frac{\gamma}{a}(\nabla^2 u)(\nabla \cdot \mathbf{m}). \qquad (15)$$

Again, this is an energy per unit volume. Similarly, the model free energy of the tilt field $\mathbf{m}$ becomes

$$f_m = \frac{1}{2a}[C_\parallel(\nabla \cdot \mathbf{m})^2 + C_\perp(\nabla \times \mathbf{m})^2 + D(\nabla^2 \mathbf{m})^2$$

$$+ t|\mathbf{m}|^2 + 2u|\mathbf{m}|^4]. \qquad (16)$$

For a stack of membranes confined between hard walls at $z = \pm L/2$, a modulation of $u(x,y,z)$ must satisfy the boundary conditions $u(x,y,z) = 0$ at $z = \pm L/2$. For thin films, we assume a single undulation mode of the form

$$u(x,y,z) = \cos(z\pi/L)u(x,y). \qquad (17)$$

The accompanying modulation of the tilt field $\mathbf{m}$ can be expressed as

$$\mathbf{m}(x,y,z) = \cos(z\pi/L)\mathbf{m}(x,y). \qquad (18)$$
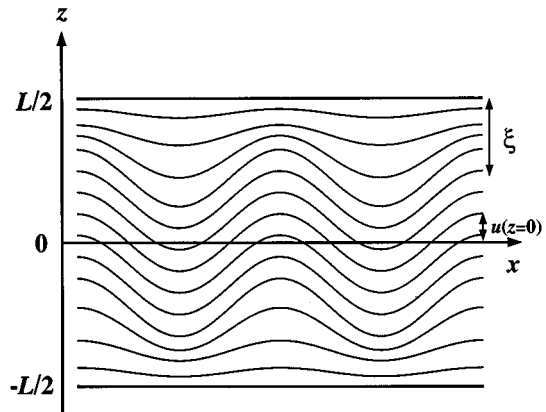

FIG. 8. A schematic illustration of the membrane shape of a smectic domain confined between walls. The amplitude of undulation $u(z)$ is uniform near $z = 0$. Due to the boundary effect, $u(z)$ decreases to zero near the boundary in a region of thickness approximately equal to the penetration depth ξ.

Here we have also assumed a single undulation mode for $u(x,y)$ and $\mathbf{m}(x,y)$. In general, for confined films of finite thickness, it is expected that the field $u(z)$ is a maximum at the center of the film ($z=0$), and that $u(z)$ decreases to zero at the boundaries ($z=\pm L/2$). For thick films, this vanishing of $u(z)$ occurs only in a finite region of thickness ξ, the penetration depth [17]. Thus, in general, there are effectively two regions in the film: (1) a bulk region near the center of the film in which the displacement $u(z)$ is constant; and (2) boundary regions near $z=\pm L/2$ only which the displacement vanishes. Near the transition from a uniform phase to a modulated phase with increasing film thickness, we expect and find that the film thickness L and penetration depth ξ are comparable. This corresponds to our single-mode approximation in Eq. (17). The general case for thicker films will be considered below, where we determine the penetration depth ξ self-consistently. In the vicinity of the point $t=C'_{\parallel}=0$, there are just two equilibrium modulated phases given by

$$m_x(x,y)=m_1\cos(qx), \qquad (19)$$

$$m_y(x,y)=m_0, \qquad (20)$$

and

$$m_x(x,y)=m_1\cos(qx), \qquad (21)$$

$$m_y(x,y)=m_1\cos(qy). \qquad (22)$$

In keeping with our previous notation, we shall refer to these as the $P^{(1)}_{\beta'}$ and the square-lattice phase. For films of finite thickness near $t=C'_{\parallel}=0$, we also find only these two modulated phases in addition to the uniform L_α and $L_{\beta'}$ phases. Note that the $P^{(1)}_{\beta'}$ phase has a nonzero average tilt of the y component $m_y(x,y,z)=m_0$ which is independent of z. Within this single-mode approximation, Eqs. (14) and (15) can be expressed as

$$\int dz(f_{\text{bulk}}+f_\gamma)=\frac{L}{4}\left(Kq^4+\bar{B}\frac{\pi^2}{L^2}\right)u^2(x,y)$$
$$+\frac{\gamma}{2a}Lq^2[\boldsymbol{\nabla}\cdot\mathbf{m}(x,y)]u(x,y). \qquad (23)$$

After replacing $u(x,y)$ by its equilibrium value, the integrated total free energy is given by

$$F=\int\int\int dxdydz(f_{\text{bulk}}+f_\gamma+f_m)$$
$$=\frac{L}{4a}\int\int dxdy\{C_{\parallel}(q)[\boldsymbol{\nabla}\cdot\mathbf{m}(x,y)]^2$$
$$+C_\perp[\boldsymbol{\nabla}\times\mathbf{m}(x,y)]^2+D[\nabla^2\mathbf{m}(x,y)]^2\}$$
$$+\frac{1}{2a}\int\int\int dxdydz[t|\mathbf{m}|^2+2u|\mathbf{m}|^4], \qquad (24)$$

where

$$C_{\parallel}(q)=C_{\parallel}-\frac{\gamma^2q^4}{[a(\bar{B}\pi^2/L^2+Kq^4)]}. \qquad (25)$$

The phase diagram near the point $t=C'_{\parallel}=0$ can be determined by comparing the free energy of L_α, $L_{\beta'}$, $P^{(1)}_{\beta'}$, and the square-lattice phase, denoted by F_α, F_β, F_1, and F_4, respectively, within the mean-field approximation. It is not difficult to find $F_\alpha=0$ and $F_\beta=-LAt^2/16ua$. In the $P^{(1)}_{\beta'}$ phase, the free energy is

$$F_1=-\frac{LA}{ua}\left(\frac{\Gamma_q^2}{20}+\frac{t^2}{16}\right), \qquad (26)$$

with $\Gamma_q=C_{\parallel}(q)q^2+Dq^4$, provided $\Gamma_q\leq0$. The wave vector q will be determined numerically by minimizing Γ_q over q. In the square-lattice phase, the free energy is

$$F_4=-\frac{LA}{30ua}(\Gamma_q+t)^2, \qquad (27)$$

provided $\Gamma_q\leq0$.

For thicker films, the inner layers are not affected by the boundary constraints. Therefore the local displacement field can be expressed as

$$u(x,y,z)=u(z)u(x,y), \qquad (28)$$

where $u(z)$ is uniform near $z=0$, and goes to zero near the boundary in a region of thickness approximately equal to the penetration depth ξ. Thus we let

$$u(z)=\begin{cases}\sin\left(\dfrac{\pi(L/2+z)}{2\xi}\right) & \text{for } -\dfrac{L}{2}\leq z\leq-\dfrac{L}{2}+\xi \\[2ex] 1 & \text{for } -\dfrac{L}{2}+\xi\leq z\leq\dfrac{L}{2}-\xi \\[2ex] \sin\left(\dfrac{\pi(L/2-z)}{2\xi}\right) & \text{for } \dfrac{L}{2}-\xi\leq z\leq\dfrac{L}{2}.\end{cases} \qquad (29)$$

The accompanying modulation of the tilt field $\mathbf{m}$ is given by

$$\mathbf{m}(x,y,z)=u(z)\mathbf{m}(x,y). \qquad (30)$$

Again, $m_y(x,y,z)=m_0$ for the $P^{(1)}_{\beta'}$ phase. Within this approximation, the free energy in Eq. (24) can be minimized over q and ξ and the phase diagram can be studied for a range of film thickness.

The phase diagram for a smectic domain confined between walls is qualitatively similar to that of the freely suspended films as shown in Fig. 9. In both cases, the undulated phases are suppressed by the boundary constraints. For a confined smectic domain, in the limit of thick samples ($L\gg\xi$), the phase diagram can be shown to be similar to that of a free membrane as described in Refs. [14,15]. For finite sample thickness ($L\approx\xi$), the square-lattice phase is unstable to the $P^{(1)}_{\beta'}$ phase because the hard-wall boundary effect disfavors the two-dimensional modulated phase. For a sample thickness less than the penetration depth, all modulated phases are unstable. In the next section, we will extend the consideration to freely suspended films and compare our predictions with experimental results.
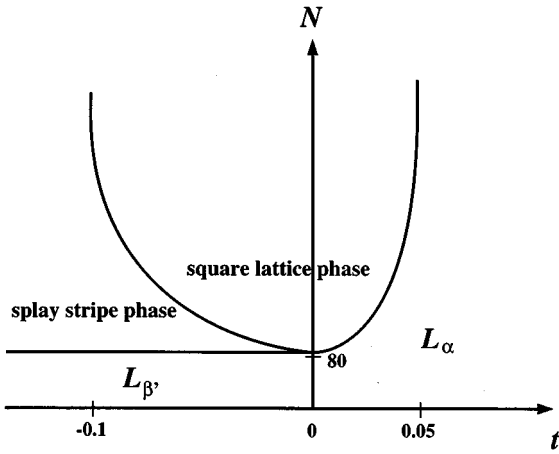
FIG. 9. The mean-field phase diagram of freely suspended films as a function of t and N. All modulated phases are suppressed by surface tension for N less than 80. The square-lattice phase occurs for N greater than 80 and for t between -0.1 and 0.05. The two flat phases are L_α (or Sm-A) and $L_{\beta'}$ (or Sm-C). The typical parameters are $K = 10^{-6}$ dyne, $\bar{B} = 2.5 \times 10^7$ dyne/cm^2, $\tau = 20$ dyne/cm, $a = 3 \times 10^{-7}$ cm, $\gamma = 2.5 \times 10^{-13}$ erg, $C_\parallel = 10^{-13}$ erg, and $D = 5 \times 10^{-26}$ erg/cm^2.

VI. FREELY SUSPENDED FILMS

In Sec. V, we have derived the phase diagram for an oriented smectic domain confined between hard walls. A similar analysis can be done for a freely suspended film. In this case, instead of the hard-wall boundary conditions, there is an excess free energy proportional to the area of the top and bottom layers of the film due to the surface tension. This excess free energy can be expressed as

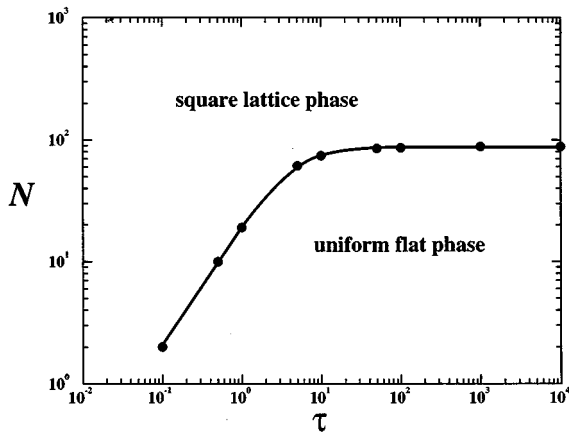$$F_\tau = \tau \int \int dx\,dy\, \frac{1}{2}(\nabla u)^2, \qquad (31)$$

FIG. 10. The mean-field phase boundary of the square-lattice phase and the uniform flat phase (L_α) as a function of the number-of-layers (N) and surface tension (τ) at $t = 0$. Above the data points, the square-lattice phase is stable, while the stable phase is the flat phase below the data points. The parameters for this figure are the following: $K = 10^{-6}$ dyne, $\bar{B} = 2.5 \times 10^7$ dyne/cm^2, $a = 3 \times 10^{-7}$ cm, $\gamma = 2.5 \times 10^{-13}$ erg, $C_\parallel = 10^{-13}$ erg, $t = 0$ dyne/cm, and $D = 5 \times 10^{-26}$ erg/cm^2.

where the integrand extends over the top and bottom surfaces. As in the case of the hard-wall boundary conditions, the surface tension also has the effect of suppressing undulations of the membranes. For thinner films, both experimental and theoretical results have indicated that the amplitude of the modulation at the surface relative to that at the center of the film decreases as the film thickness L is increased [28, 29]. Therefore we assume a single undulation mode of the form

$$u(x,y,z) = \cos(z\pi/L')u(x,y). \qquad (32)$$

The accompanying modulation of the tilt field $\mathbf{m}$ is of the form

$$\mathbf{m}(x,y,z) = \cos(z\pi/L')\mathbf{m}(x,y). \qquad (33)$$

Here L' characterizes the decay in the z direction. This is essentially a penetration depth. We let $L = \alpha L'$, where $0 \le \alpha \le 1$. Here $\alpha = 0$ corresponds to a film that is uniform in the z direction. This is expected for either very thin films or for vanishing surface tension. On the other hand, $\alpha = 1$ corresponds to a complete vanishing of the modulation at the surfaces $z = \pm L/2$. This is expected for thick films or for high surface tensions. The total free energy of the film can be calculated as

$$F_{\text{tot}} = F_\tau + F = \frac{L'}{2a\pi}\left[\frac{\alpha\pi}{2} + \cos\left(\frac{\alpha\pi}{2}\right)\sin\left(\frac{\alpha\pi}{2}\right)\right]$$
$$\times \int \int dx\,dy\{C_\parallel(q)[\nabla \cdot \mathbf{m}(x,y)]^2$$
$$+ C_\perp[\nabla \times \mathbf{m}(x,y)]^2 + D[\nabla^2\mathbf{m}(x,y)]^2\}$$
$$+ \frac{1}{2a}\int \int \int dx\,dy\,dz(t|\mathbf{m}|^2 + 2u|\mathbf{m}|^4), \qquad (34)$$

with

$$C_\parallel(q) = C_\parallel - \frac{\gamma^2 q^4 L'\left[\frac{\alpha\pi}{2} + \cos\left(\frac{\alpha\pi}{2}\right)\sin\left(\frac{\alpha\pi}{2}\right)\right]}{[a\pi(g_B + g_K + g_\tau)]}, \qquad (35)$$

where

$$g_B = \frac{\bar{B}\pi}{L'}\left[\frac{\alpha\pi}{2} - \cos\left(\frac{\alpha\pi}{2}\right)\sin\left(\frac{\alpha\pi}{2}\right)\right], \qquad (36)$$

$$g_K = \frac{KL'q^4}{\pi}\left[\frac{\alpha\pi}{2} + \cos\left(\frac{\alpha\pi}{2}\right)\sin\left(\frac{\alpha\pi}{2}\right)\right], \qquad (37)$$

and

$$g_\tau = 2\tau q^2 \cos^2\left(\frac{\alpha\pi}{2}\right). \qquad (38)$$

In the limit of thin films, α is small and the undulation of the film becomes

$$u(x,y,z) = u(x,y), \qquad (39)$$

which is independent of z. The total free energy then becomes

$$F_{\text{tot}} = \frac{L}{2a} \int \int dxdy \{C_\parallel(q)[\boldsymbol{\nabla} \cdot \mathbf{m}(x,y)]^2 + C_\perp[\boldsymbol{\nabla} \times \mathbf{m}(x,y)]^2$$
$$+ D[\nabla^2 \mathbf{m}(x,y)]^2 + t|\mathbf{m}(x,y)|^2 + 2u|\mathbf{m}(x,y)|^4\} \quad (40)$$

with

$$C_\parallel(q) = C_\parallel - \gamma^2 q^4 / [a(2\tau q^2/L + Kq^4)]. \quad (41)$$

For large surface tension τ, it can be shown that there are no stable modulated phases in thin films because the surface energy dominates the free energy. However, for small surface tensions, the transition from the uniform flat phase to modulated phases occurs when $N > N_1 = 8D\tau\gamma^2/(a^2 K^2 C_\parallel'^2)$ for $t \cong 0$.

For thicker films, within the above approximation, we calculate the free energy for various modulated phases. In the $P_{\beta'}^{(1)}$ phase, the free energy is given by

$$F_1 = -\frac{LA}{16ua} \left\{ \frac{\left[1 + \frac{2}{\alpha\pi}\cos\left(\frac{\alpha\pi}{2}\right)\sin\left(\frac{\alpha\pi}{2}\right)\right]^2 \Gamma_q^2}{\left\{\frac{9}{4} + \frac{3}{\alpha\pi}\cos\left(\frac{\alpha\pi}{2}\right)\sin\left(\frac{\alpha\pi}{2}\right)\left[\cos^2\left(\frac{\alpha\pi}{2}\right) + \frac{3}{2}\right]\right\} - \left[1 + \frac{2}{\alpha\pi}\cos\left(\frac{\alpha\pi}{2}\right)\sin\left(\frac{\alpha\pi}{2}\right)\right]^2} + t^2 \right\}, \quad (42)$$

provided $\Gamma_q \le 0$. In the square-lattice phase, the free energy is given by

$$F_4 = -\frac{LA}{40ua} \frac{\left[1 + \frac{2}{\alpha\pi}\cos\left(\frac{\alpha\pi}{2}\right)\sin\left(\frac{\alpha\pi}{2}\right)\right]^2 (\Gamma_q + t)^2}{\left[\frac{3}{4} + \frac{1}{\alpha\pi}\cos^3\left(\frac{\alpha\pi}{2}\right)\sin\left(\frac{\alpha\pi}{2}\right) + \frac{3}{2\alpha\pi}\cos\left(\frac{\alpha\pi}{2}\right)\sin\left(\frac{\alpha\pi}{2}\right)\right]}, \quad (43)$$

provided $\Gamma_q \le 0$.

In general, the phase diagram can be calculated using the free energy in Eqs. (42) and (43) together with suitable boundary conditions. In the presence of nonvanishing curvatures and finite surface tension at the boundaries, the stress of the layers must balance the Laplace pressure [17]. This boundary condition can be expressed as

$$\bar{B}\left(\frac{\partial u}{\partial z}\right) = \tau\nabla^2 u. \quad (44)$$

After substitution of Eq. (32) into Eq. (44), the boundary condition becomes

$$\frac{\alpha\pi}{2}\tan\left(\frac{\alpha\pi}{2}\right) = \frac{Lq^2\tau}{2\bar{B}}. \quad (45)$$

We note that the above boundary condition is equivalent to minimizing the free energy in Eq. (34) with respect to α. The phase diagram in Fig. 9 is obtained using the following representative parameters: $K = \kappa/a = 10^{-6}$ dyne, $\bar{B} = 2.5 \times 10^7$ dyne/cm^2, $\tau = 20$ dyne/cm, $a = 3 \times 10^{-7}$ cm, $\gamma = 2.5 \times 10^{-13}$ erg, and $C_\parallel = 10^{-13}$ erg. These values correspond to the smectic phase that is unstable to modulation in the bulk near $t = 0$. We have chosen $\gamma \approx C_\parallel \approx \kappa = Ka$ as expected [30]. We further choose $D = 5 \times 10^{-26}$ erg/cm^2 in order to obtain $q \approx 10^6$ cm^{-1} as observed in the modulated phases of Ref. [13].

We compare our results with experimental data for the liquid crystal 4-n-heptyloxybenzylidene-4-n-heptylaniline (7O.7). The phase diagram of 7O.7 as a function of temperature and film thickness has been thoroughly studied [13,31].

For the above parameters, we estimate that the transition from a uniform flat phase to the square-lattice phase occurs at about 10–100 layers with a undulation wave vector q of about 10^6 cm^{-1}. The square-lattice phase exists in a region of temperature range of order a few degrees C. These results agree qualitatively with the experimental data from Ref. [13].

Furthermore, we calculate the dependence of the phase boundary between the uniform flat phase and the square-lattice phase on surface tension (τ) and compression modulus ($\bar{B}$) at $t \cong 0$. This is done numerically for the square-lattice phase and the uniform flat phase with the above parameters. The phase boundary is given by the condition $\Gamma_q = 0$. In Fig. 10, we plot the phase boundary as a function of N and surface tension τ. As shown in Fig. 10, for small surface tensions, N grows linearly as τ increases. For large surface tensions, however, the phase boundary is independent of τ. This is due to the suppression of the surface undulation by the large surface tension, and therefore the competition between compression energy and undulation energy will determine the ground state. For large surface tensions, the phase boundary is approximately given by $L \sim \xi$, where $\xi \simeq q^{-2}\sqrt{\bar{B}/K}$ is the penetration depth for a mode of the wave vector q in the x-y plane. Thus the number of layers at the phase boundary for the small compression modulus is found to scale as $N \sim \sqrt{\bar{B}}$. Assuming that the number of layers N at the transition can be characterized by a single combination of $\bar{B}$ and τ, we write

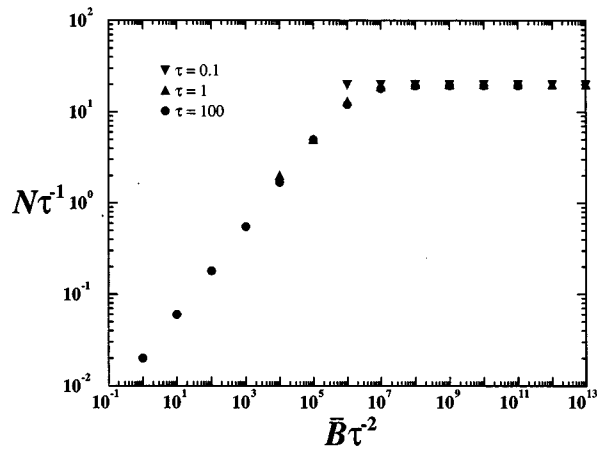$$N \sim \tau g(\bar{B}\tau^{-x}), \quad (46)$$

FIG. 11. The rescaled mean-field phase boundary of the square-lattice phase and the uniform flat phase (L_α) as a function of N/τ and $\bar{B}/\tau^2$. Above the data points, the square-lattice phase is stable, while the stable phase is the flat phase below the data points. For the different values of the surface tension τ, the rescaled curves of the phase boundary are the same. This data collapse illustrates the scaling $N \sim \tau g(\bar{B}/\tau^2)$. The parameters for this figure are the following: $K = 10^{-6}$ dyne, $a = 3 \times 10^{-7}$ cm, $\gamma = 2.5 \times 10^{-13}$ erg, $C_\parallel = 10^{-13}$ erg, $t = 0$ dyne/cm, and $D = 5 \times 10^{-26}$ erg/cm^2.

where g is a scaling function. From the limit above, we find that $g(y) \sim \sqrt{y}$ for small y, and $g(y) \sim$ constant for large y. Thus we expect $x = 2$ and

$$N \sim \tau g(\bar{B}/\tau^2). \tag{47}$$

In Fig. 11 we plot N/τ vs $\bar{B}/\tau^2$ and find a simple scaling curve for various values of τ.

VII. DISCUSSION

In this paper, we have examined the effects of boundaries on modulated phases of liquid crystal films and lipid bilayer membranes. For freely suspended films, we find that our model is consistent with the experimental observation of the phase transitions from uniform to square-lattice modulated structures for films thicker than approximately 100 layers [13]. We note, however, that our model treats only the ori-

entational (tilt) order within the films. The systems studied in Ref. [13] exhibit not only smectic-C phases, but also crystalline phases. However, to the extent that the characteristic wavelengths of the various modulated phases are large compared with the molecular size, we expect that our results can be applied to understand the modulated phases.

Our model is a phenomenological one. Thus a direct comparison of the phase diagram in Fig. 9 with the experiments of Ref. [13] is not possible. In particular, we note that the observation of the square-lattice phase between a high-temperature one-dimensional rippled phase and a low-temperature flat crystalline phase is not accounted for by our model. Nevertheless our model can help to explain the appearance of a square-lattice modulated phase rather than a hexagonal phase. The square-lattice phase is a possible stable equilibrium phase that maintains the inversion symmetry of the film.

This inversion symmetry can be broken by, among other things, an applied electric field perpendicular to the plane of the film. In this case we find that for strong fields an equilibrium hexagonal phase is predicted. However we also find an interesting result that the transition from the square-lattice phase to the hexagonal phase occurs continuously, rather than via a first-order reconstruction. Between the square-lattice phase and the hexagonal phase is an intermediate phase of lower symmetry than either of the other two. This situation is analogous to what happens in certain uniform tilted smectics. Between the smectic-I and smectic-F phases, both of which are achiral, an intermediate smectic-L phase can occur, which is chiral [1,32]. The transitions are second order. It should be possible to observe at least the continuous distortion of the square-lattice phase in films such as those studied in Ref. [13] in the presence of a transverse electric field. Depending on the strength of the flexoelectric effect in such systems, the continuous transition to the hexagonal phase at high fields may also be possible.

[1] E.B Sirota, G.S Smith, C.R. Safinya, R.J. Plano, and N.A. Clark, Science **242**, 1406 (1988).

[2] A. Tardieu, V. Luzzati, and F.C. Reman, J. Mol. Biol. **75**, 711 (1973).

[3] M.J. Janiak, D.M. Small, and G.G. Shipley, Biochemistry **15**, 4575 (1976).

[4] E.J. Luna and H.M. McConnell, Biochim. Biophys. Acta **466**, 381 (1977).

[5] J.A.N. Zasadzinski, J. Schneir, J. Gurley, V. Elings, and P.K. Hansma, Science **239**, 1013 (1988).

[6] D.C. Wack and W.W. Webb, Phys. Rev. Lett. **61**, 1210 (1988).

[7] Anomalous elasticity of such a membrane has recently been

studied in J. Toner, Phys. Rev. Lett. **74**, 415 (1995).

[8] R.B. Meyer, L. Liebert, L. Strzelecki, and P. Keller, J. Phys. (Paris) **36**, L69 (1975); J. Maclennan, Europhys. Lett. **13**, 435 (1990).

[9] S.A. Langer and J.P. Sethna, Phys. Rev. A **34**, 5035 (1986).

[10] T.J. Scheffer, H. Gruler, and G. Meier, Solid State Commun. **11**, 253 (1972).

[11] R.B. Meyer and P.S. Pershan, Solid State Commun. **13**, 989 (1973).

[12] G.A. Hinshaw, Jr. and R.G. Petschek, Phys. Rev. B **37**, 2133 (1987); G.A. Hinshaw, R.G. Petschek, and R.A. Pelcovits, Phys. Rev. Lett. **60**, 1864 (1988); G.A. Hinshaw, Jr. and R.G. Petschek, Phys. Rev. A **39**, 5914 (1989).

[13] E.B. Sirota, P.S. Pershan, and M. Deutsch, Phys. Rev. A **36**, 2902 (1987).

[14] T.C. Lubensky and F.C. MacKintosh, Phys. Rev. Lett. **71**, 1565 (1993).

[15] C.-M. Chen, T.C. Lubensky, and F.C. MacKintosh, Phys. Rev. E **51**, 504 (1995).

[16] C.-M. Chen and F.C. MacKintosh, Europhys. Lett. **30**, 215 (1995).

[17] P.G. de Gennes and J. Prost, *The Physics of Liquid Crystals* (Oxford, London, 1993).

[18] D. Blankschtein and R.M. Hornreich, Phys. Rev. B **32**, 3214 (1985).

[19] W. Helfrich and J. Prost, Phys. Rev. A **38**, 3065 (1988).

[20] A.E. Jacobs, G. Goldner, and D. Mukamel, Phys. Rev. A **45**, 5783 (1992).

[21] R.B. Meyer, Phys. Rev. Lett. **22**, 918 (1969).

[22] W. Helfrich, Mol. Cryst. **26**, 1 (1974).

[23] J. Prost and J.P. Marcerou, J. Phys. (Paris) **38**, 315 (1977).

[24] J.P. Marcerou and J. Prost, Mol. Cryst. Liq. Cryst. **58**, 259 (1980).

[25] M.M. Standish and B.A. Pethica, Trans. Faraday Soc. **64**, 1113 (1968).

[26] J.C.W. Shepherd and G. Bueldt, Biochim. Biophys. Acta **514**, 83 (1978).

[27] H.L. Scott and C.Y. Lee, J. Chem. Phys. **73**, 5351 (1980).

[28] R. Holyst, D.J. Tweet, and L.B. Sorensen, Phys. Rev. Lett. **65**, 2153 (1990); D.J. Tweet, R. Holyst, B.D. Swanson, H. Stragier, and L.B. Sorensen, *ibid.* **65**, 2157 (1990).

[29] F.C. MacKintosh, Phys. Rev. E **50**, 2891 (1994).

[30] F.C. MacKintosh and T.C. Lubensky, Phys. Rev. Lett. **67**, 1169 (1991).

[31] J. Collete, P.S. Pershan, E.B. Sirota, and L.B. Sorensen, Phys. Rev. Lett. **52**, 356 (1984); E.B. Sirota, P.S. Pershan, L.B. Sorensen, and J. Collett, *ibid.* **55**, 2039 (1985); Phys. Rev. A **36**, 2890 (1987).

[32] J.V. Selinger and D.R. Nelson, Phys. Rev. A **39**, 3135 (1989).